Isolating the impacts of urban form and fabric from geography on urban heat and human thermal comfort

Kerry A. Nice[a,*], Negin Nazarian[b,c], Mathew J. Lipson[b], Melissa A. Hart[b], Sachith Seneviratne[a], Jason Thompson[a], Marzie Naserikia[b], Branislava Godic[a], Mark Stevenson[a,d]

[a]*Transport, Health, and Urban Design Research Lab, Faculty of Architecture, Building, and Planning, University of Melbourne, VIC, Australia.*
[b]*ARC Centre of Excellence for Climate Extremes, University of New South Wales, Sydney, NSW, Australia.*
[c]*School of Built Environment; and City Futures Research Centre, University of New South Wales, Sydney, NSW, Australia.*
[d]*Melbourne School of Engineering; and Melbourne School of Population and Global Health, University of Melbourne, VIC, Australia.*

Abstract

Public health risks resulting from urban heat in cities are increasing due to rapid urbanisation and climate change, motivating closer attention to urban heat mitigation and adaptation strategies that enable climate-sensitive urban design and development. These strategies incorporate four key factors influencing heat stress in cities: the urban form (morphology of vegetated and built surfaces), urban fabric, urban function (including human activities), and background climate and regional geographic settings (e.g. topography and distance to water bodies). The first two factors can be modified and redesigned as urban heat mitigation strategies (e.g. changing the albedo of surfaces, replacing hard surfaces with pervious vegetated surfaces, or increasing canopy cover). Regional geographical settings of cities, on the other hand, cannot be modified and while human activities can be modified, it often requires holistic behavioural and policy modifications and the impacts of these can be difficult to quantify. When evaluating the effectiveness of urban heat mitigation strategies in observational or traditional modelling studies, it can be difficult to separate the impacts of modifications to the built and natural forms from the interactions of the geographic influences, limiting the universality of results. To address this, we introduce a new methodology to determine the influence of urban form and fabric on thermal comfort, by utilising a comprehensive combination of possible urban forms, an urban morphology data source, and micro-climate modelling. We perform 9814 simulations covering a wide range of realistic built and natural forms (building, roads, grass, and tree densities as well as building and tree heights) to determine their importance and influence on thermal environments in urban canyons without geographical influences. We show that higher daytime air temperatures and thermal comfort indices are strongly driven by increased street fractions, with maximum air temperatures increases of up to 10 and 15°C as street fractions increase from 10% (very narrow street canyons and/or extensive vegetation cover) to 80 and 90% (wide street canyons). Up to 5°C reductions in daytime air temperatures are seen with increasing grass and tree fractions from zero (fully urban) to complete (fully natural) coverage. Similar patterns are seen with the Universal Thermal Climate Index (UTCI), with increasing street fractions of 80% and 90% driving increases of 6 and 12°C, respectively. We then apply the results at a city-wide scale, generating heat maps of several Australian cities showing the impacts of present day urban form and fabric. The resulting method allows mitigation strategies to be tested on modifiable urban form factors isolated from geography, topography, and local weather conditions, factors that cannot easily be modified.

Keywords: micro-climate modelling, urban morphology, heat mitigation, urban heat

1. Introduction

1.1. Need for urban heat mitigation measures

Measures of cumulative heat show significant increases in recent decades with trends of increased heatwave frequency and duration seen globally (Perkins-Kirkpatrick and Lewis, 2020). Exposure to dangerous levels of heat stress

*Principal corresponding author
Email address: kerry.nice@unimelb.edu.au (Kerry A. Nice)

may increase by a factor of 5-10 by 2080 (Coffel et al., 2018), driven by more frequent, severe, and long-lasting heatwaves (IPCC, 2022). Heat is the most dangerous natural hazard in many places in the world, including Australia (Coates et al., 2014) and Europe (Forzieri et al., 2017), with disproportionate risks falling on vulnerable populations such as elderly and the very young (Nicholls et al., 2008).

The design of cities has exacerbated the risks associated with heat extremes. Urbanisation replaces natural pervious land covers with hard heat-absorbent surfaces, altering the surface energy balance in cities (Oke, 1982). Anthropogenic waste heat from buildings and transport as well as shadowing and radiation trapping within the urban canopy result in larger amounts of net energy at street level. Meanwhile, the conversion of vegetated to impervious surfaces, and the reduction of available water in cities, shifts the urban energy balance away from latent heat (water evaporation) towards increased sensible heat (heat that can be felt) and increased heat storage in urban surfaces. Collectively, the modification of the urban energy balance result in higher canopy air and surface temperatures in the built environments compared to natural land covers, exacerbating heat stress risks for inhabitants (Coutts et al., 2012; Martilli et al., 2020).

Reviewing the influence of cities on local meteorology, urban climates are influenced by four key factors: 1) urban form (morphology of vegetated and built surfaces), 2) urban fabric (built materials as well as the natural and vegetated cover, i.e., soil, water, vegetation and their phenology), 3) urban functions (influencing emissions of heat, moisture and pollutants released by human activities), and 4) background climate and regional geography (Masson et al., 2020b; Mills et al., 2021). Urban heat mitigation strategies consider a combination of these factors in planning and design of urban developments, aiming to address the adverse effects of urban design on the thermal environment. These strategies, which often rely on modifications to urban form and fabric in cities, require both an understanding of the processes driving excess heat, and the methods required to identify the existing areas of high risk that will benefit most from interventions. In a systematic review of mitigation strategies, Krayenhoff et al. (2021) assessed the performance of cooling strategies (determined through numerical modelling) and identified commonly-used urban heat mitigation strategies including cooling through albedo changes, vegetation cover, irrigation and water, and photovoltaic panels. Albedo changes (i.e., increasing the reflectivity of urban surfaces) can reduce road and sidewalk surface temperatures but may cause increased radiant loads for pedestrians (Middel et al., 2020). If applied at roof levels, albedo changes can provide urban heat reductions (Jacobs et al., 2018). Urban vegetation provides cooling benefits through shading of urban surfaces and evapotranspiration (Bowler et al., 2010; Coutts et al., 2012, 2015), as well as reducing hard impervious surfaces in favour of pervious vegetated surfaces (Middel and Krayenhoff, 2019). Additional cooling can also be realised through irrigation of both vegetated (Broadbent et al., 2017; Cheung et al., 2021) and impervious surfaces (Hendel et al., 2016; Solcerova et al., 2018).

These studies are critical in understanding the impact of urban design in reducing canopy air temperature and minimising the negative impacts of heat exposure on urban dwellers. However, assessments of mitigation effectiveness often rely on specific use cases and model scales (Krayenhoff et al., 2021). More importantly, the interaction of the different elements of urban form, as well as the compounding effect on canopy temperatures and heat stress, are often non-linear, which is often not represented in observational or modelling analyses of mitigation strategies. Most studies consider the performance of varying one design parameter at a time, while in reality, urban form and fabric parameters are changing interdependently. In realistic urban settings, the compounding effects of various urban form and fabric metrics modulate the impact of other mitigation strategies, which is often overlooked in the literature. The complexity of these interactions makes quantifying the impact of each mitigation measure difficult across different cities and their individual mixes of urban forms. Lastly, each city's regional geography (including topography and distance from and orientation to water bodies) adds additional complexity in separating the impact of mitigation measures from the influences of background climates, questioning the scalability of findings to other scenarios and cities. The present study is motivated by the shortcomings of existing methods in assessing the performance of mitigation strategies in realistic urban settings, where multi-dimensional changes in urban form and fabric often occur. Furthermore, we aim to isolate the impact of urban form and fabric from geography such that we better understand the relative contribution of various design factors to urban heat and human thermal comfort.

1.2. Comprehensive analyses of urban form and fabric to inform urban heat mitigation strategies

Numerical modelling can be used to assess changes in thermal conditions resulting from modifications to urban form and fabric, and calculate thermal comfort indices such as the Universal Thermal Climate Index ($UTCI$) (Bröde et al., 2012) at different temporal and spatial scales. To ensure accurate and representative analyses, however, urban

climate modelling should follow key requirements identified by Masson et al. (2020a) and Krayenhoff et al. (2021): appropriate modelling scale, fit-for-purpose model physics with validated sub-models, and appropriate descriptive data of urban areas. Addressing these three pillars, here we describe not only the scale, resolution, and suitability of the model for urban heat and human thermal comfort analyses, but draw attention to city-description datasets that can depict realistic, multi-dimensional variation in urban form and fabric.

Resolving interactions between local urban features and broader meteorological processes requires modelling at meso or larger scales, where computational constraints typically necessitate the representation of cities as simplified and idealised (e.g., 2-dimensional) versions of the urban 3D geometry (Masson, 2005). These methods can be used to assess strategies which affect variables such as above roof air temperature. Human thermal comfort modelling, on the other hand, needs to be undertaken in 3-dimensions at a micro-scale resolution, thereby accounting for the influence of shading, vegetation, and water features. Examples of models at this scale that account for vegetation impacts and urban hydrology, or that can explicitly calculate parameters needed to estimate human thermal comfort, include: ENVI-met (Bruse, 1999), VTUF-3D (Nice et al., 2018), SOLWEIG/UMEP (Lindberg et al., 2018), PALM-4U (Dominik and Andreas, 2019; Hettrich et al., 2020), CAT (Erell and Williamson, 2006), and OTC3D (Nazarian et al., 2017, 2018). In this study VTUF-3D is used to assess the contribution of urban form and fabric to air temperature and thermal comfort. VTUF-3D is a validated surface energy balance micro-climate model that accounts for the distribution of radiative fluxes between surfaces in an explicit 3-dimensional urban canyon representation, which is critical for thermal comfort analyses. It can also account for the impacts of vegetation shading and evapotranspiration, producing high-resolution predictions of surface temperatures, mean radiant temperature, and $UTCI$, allowing us to assess the compounding contribution of and fabric on canopy temperature and human thermal comfort.

A comprehensive set of sensitivity analyses covering the full range of realistic built and natural forms in cities can be used to isolate the influence of the city form and fabric from the geography. Previously, analyses such as these have been limited to a class-based assessment, where Local Climate Zone (LCZ) classifications are introduced to characterise the physical nature of cities. LCZ classifications provide the urban form input for climate modelling of specific areas (Stewart et al., 2014; Verdonck et al., 2018; Hammerberg et al., 2018; Masson et al., 2020a; Emery et al., 2021) and has been used to describe the variability in remote sensed surface temperatures (Alexander, 2021; Li et al., 2022; Peng et al., 2022), or high-resolution air temperatures observations (Milošević et al., 2016; Skarbit et al., 2017; Top et al., 2020; Potgieter et al., 2021). However, the range of urban parameters for each class can be quite broad. For example, for the LCZ6 class (the open low-rise typology), impervious surface fractions can range from 20-50% and pervious of 30-60%. As the results of this study will show, significant differences in thermal outcomes can be seen across these ranges. To address this, a pathway has been planned (Ching et al., 2019) using satellite imagery and OpenStreetMap to refine the land cover resolution to 2m and provide a complete set of urban canopy parameters needed for modelling, including building heights and footprints, and catalogues of urban form typologies (material types and properties, vegetation types, and building ages). Other sources of urban information are also becoming available, such as the commercial provider Geoscape (Geoscape, 2020), which provides 2m resolution land cover coverage, as well as building and tree heights and footprints, of all Australian urban areas. Considering the emerging trends in global cities to provide such high-resolution information to describe urban environments, this dataset (Geoscape) is used here to represent the realistic variability in urban form and fabric at micro-scales.

This study will generate a comprehensive set of thousands of possible urban form combinations and individually model each of those using a micro-scale modelling approach with VTUF-3D. This analyses will quantify both the relative influence of each surface type in the urban mix and the sensitivity of canopy temperatures and $UTCI$ to a combination of design parameters. As an application example, the results from each combination of urban form and fabric will be applied back to individual locations, as determined by high resolution Geoscape data, to provide a micro-scaled thermal comfort map of a large urban area. This approach allows the isolation of the effects of local urban form from influences present in larger-scale modelling, such as regional climate, topography, and coastal breezes.

In summary, we introduce a methodology to determine the influence of urban form and fabric on thermal comfort, by utilising a comprehensive combination of possible urban forms, an urban morphology data source, and micro-climate modelling. The proposed analyses will then follow three key objectives: 1) model the full range of representative combinations of urban form (mixes of land cover and urban and vegetative structure) at a micro-scale (Section 2), 2) determine the importance and relative influence of each feature type on thermal performance (Section 3), and 3) discuss how the results can be extended to a city-wide assessment of thermal comfort such that we identify areas that may benefit from heat mitigation interventions (Section 4). The proposed methodology will inform future research in

planning and development of realistic strategies for urban heat mitigation.

2. Methods

The overall workflow for this project is presented in Figure 1. Each step is detailed in the following sections.

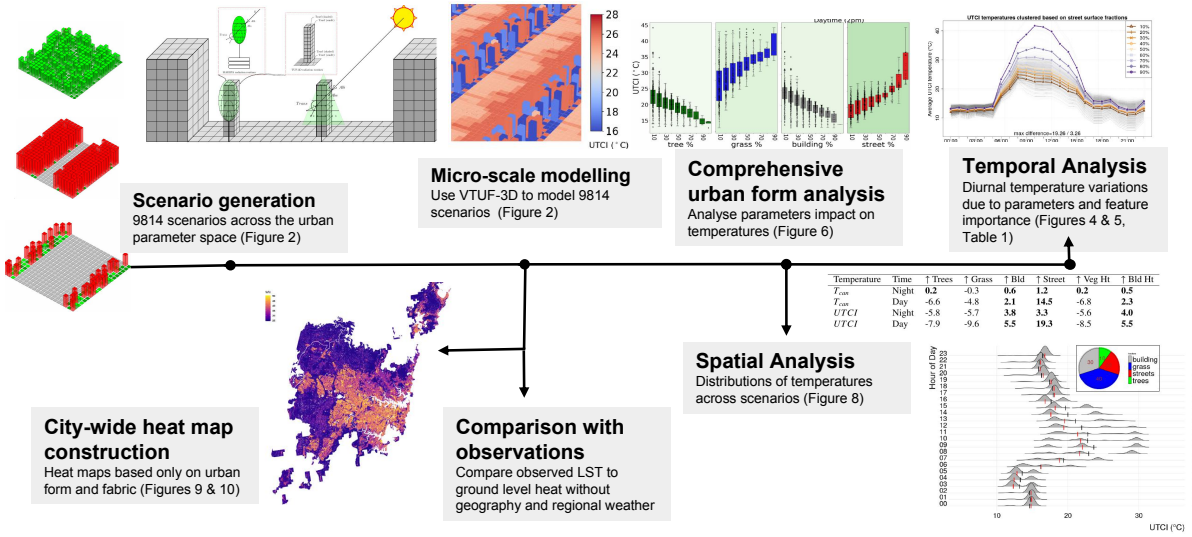

Figure 1: **Workflow flow for this project.**

2.1. Scenario generation

Modelling domains of 100×100m with 5m resolutions were created by iterating through all fractions of trees, grass, buildings and streets (in 5% increments), as well as heights (in 0.5m increments) of buildings (from 0 to 50 meters) and vegetation (from 0 to 20 meters). Schematics of a few simulation scenarios are shown in Figure 2. In the example shown in Figure 2b, the domain consists of 60% buildings, 31% streets, 9% grass, and 0% trees and the average building height (across the entire domain) of 49.8m and average tree height of 0.0m. Multiple variations using the same surface fractions are created as heights are iterated from 0m to 50m for building and 0m to 20m for trees. This resulted in 9814 scenarios.

Heights of individual buildings and trees could reach the maximum heights but heights and locations were weighted to achieve a specific sky view factor (as related to average domain heights). Average heights can be calculated in two different ways. For example, in the scenario in Figure 2b, the average building height (of only the buildings) is 49.8m. However, the metric used in this project will be an average calculated across the entire area of the domain producing, in this case, an average building height of 30.0m. Note, the distribution of surface types were intended to resemble an urban canyon unit starting with a road through the middle and other types distributed on either side. See Supplementary Figure S5 showing the distribution of surface fractions across all the modelled domains.

2.2. VTUF-3D

VTUF-3D (Nice et al., 2018) was used as the micro-climate modelling tool for this study. VTUF-3D is an urban micro-climate surface energy balance model that incorporates vegetation physiological processes and shading effects. Few urban micro-climate models are available that account for vegetation and that run at high resolutions. SOLWEIG only accounts for the shade of the vegetation. Others such as ENVI-met or PALM-4U are highly computationally intensive, making running thousands of scenarios impractical. However, VTUF-3D is computationally efficient enough to allow thousands of high resolution simulations to be run with appropriate accuracy. The model provides output of a canyon averaged air temperature (T_{can}) as well as spatial 3-dimensional values for surface temperature (T_{sfc}), mean radiant temperature (T_{mrt}), and the Universal Thermal Climate Index ($UTCI$) (Figure 2d). The model can deliver any

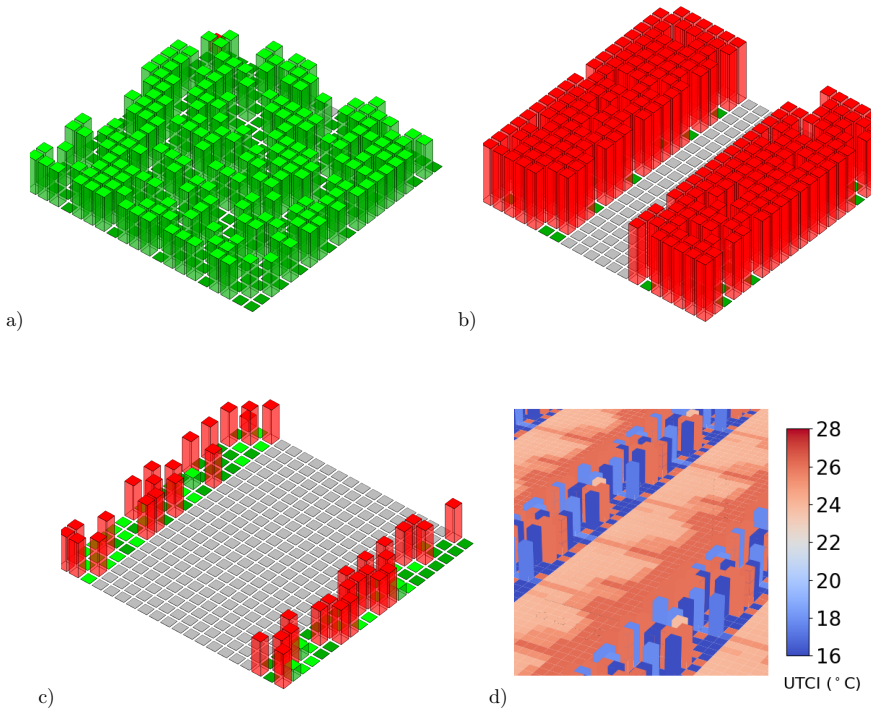

Figure 2: **Three example scenarios from the 9814 modelled in the project, a) 49% grass, 50% trees, 0.5% roads, 0.5% building, mean building height 5.0m, mean vegetation height 15.0m (7.5m averaged across domain), b) 9% grass, 0% trees, 31% roads, 60% building, mean building height 49.8m (30.0m averaged across domain), mean vegetation height 0m, c) 9% grass, 10% trees, 71% roads, 10% building, mean building height 14.8m (1.5m averaged across domain), mean vegetation height 0.5m. Building heights are given as average heights of buildings (and an area-weighted average building height). Vegetation heights follow the same pattern. d) Modelled 3-dimensional results of $UTCI$ for scenario (c) at 2pm February 12, 2004. Note, VTUF-3D nests a central area of interest in 9 identical surrounding areas and this visualisation includes some of these surrounding nested results.**

level of resolution but in this study scenarios were run with a 5m resolution. The scenarios were forced by observations from Preston in Melbourne from Coutts et al. (2007) over the five days February 9-13, 2004. The VTUF-3D model has undergone a comprehensive validation process (Nice, 2016; Nice et al., 2018) using this forcing data.

In these validations, comparisons of modelled fluxes to observed found that latent energy was often underestimated during the daytime as well as a slight over-estimation of ground heat fluxes at midday. When compared to results from the Best and Grimmond (2012) International Urban Land-Surface Model Comparison project, VTUF-3D had lower RMSE values for all fluxes besides latent energy when compared to other models with integrated vegetation modelling, so performs well in comparison to comparable surface energy balance models. When evaluating VTUF-3D's predictions of T_{mrt} and $UTCI$, VTUF-3D showed a slight delay in warming during the mornings compared to observations of T_{mrt} and $UTCI$ was 1-2°C too cold during the night and early mornings. Validations of air temperature are difficult as VTUF-3D generates canyon averaged air temperatures which are not entirely comparable to single point observations. In the validations, VTUF-3D over-estimated air temperatures by 1-2°C during the warmest part of the day. However, the relative differences in air temperatures between urban streets with low amounts of tree canopy cover and those with much more extensive cover was in good agreement with the observations of Coutts et al. (2015). The implications of these validations for this study are that temporal patterns of heating might be delayed compared to observed values. VTUF-3D may overestimate absolute values of air temperature but will be in better agreement when comparing relative values between scenarios of varying land covers. Finally, the absolute values predicted for $UTCI$ might be colder at night than in urban areas. A further limitation of VTUF-3D is it is an offline model, meaning the forcing weather data is not responsive to changes at the surface and do not influence the ongoing weather conditions. When using a recent version of TUF-3D (for which an earlier version was used as the foundation for VTUF-3D), Stewart et al. (2021) found offline modelling wasn't a large factor with surface temperatures but can have some impact on air temperatures. Surface temperatures are an important contributor in the calculation of T_{mrt} and $UTCI$ temperatures.

February 12, 2004 was chosen as a comparison day for the analysis. The forcing data for this day is presented in Figure 3. Air temperatures on this day reached 26°C, which is close to the climatological mean maximum temperature for Melbourne (25.8°C). February 12th was chosen as a representative warm summer day with clear sky conditions across the entire day. The combination of air temperature and incoming shortwave radiation caused some periods of heat stress. Many heat mitigation assessments concentrate on extreme heat days, however, in cities like Melbourne, even days close to the climatological mean can cause levels of heat stress, especially within some urban morphologies (i.e. large amounts of unshaded impervious surfaces). Further, the number of days similar to February 12th, where some level of heat stress and thermal discomfort can be experienced, far exceed the number of extreme heat days. For example, in Melbourne over 2015-2020, the average number of days per year that exceed 35°C are 11 compared to 80 days per year that exceed 25°C (Bureau of Meteorology, 2021).

2.3. Comprehensive urban form analysis

To determine the influence of each urban form parameter on heat stress and thermal conditions, a sensitivity analysis was performed on the full range of parameters (fractions of grass, street, building, and vegetation as well as average vegetation and building heights). VTUF-3D generates a single canyon averaged air temperature (T_{can}), therefore a single (well mixed) air temperature value was extracted for each timestep from the 9814 completed model runs. Additional temperature results are spatially distributed in 3-dimensions across all the surfaces in the scenario. A slice at 0m (ground level) was extracted for $UTCI$ and a domain mean value calculated for each timestep for each scenario. Full 3-dimensional results were also extracted for later use in Section 4.2. Mean temperatures, clustered by fraction percentages and heights in 10% increments of surface fractions or 0.8 meter average heights, were calculated for T_{can} and $UTCI$ across the representative day of February 12, 2004 and the trends analysed over the different fraction clusters and over the diurnal cycle.

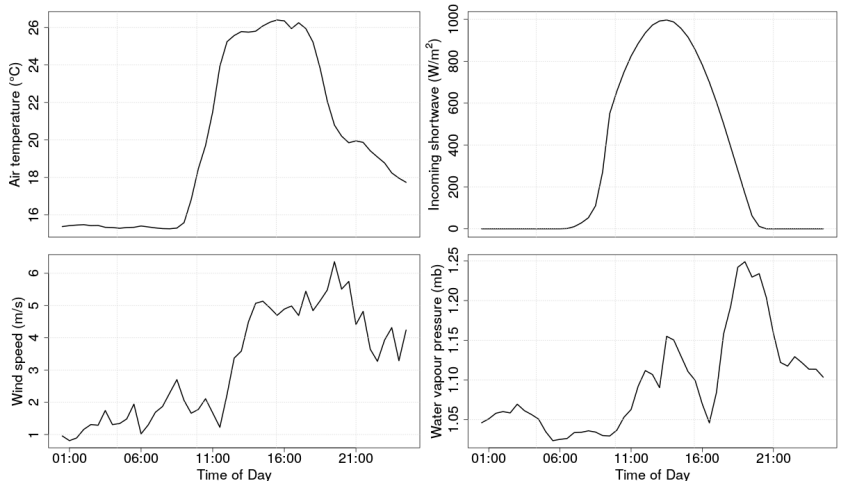

Figure 3: **Forcing data (air temperature, incoming shortwave, wind speed, and water vapour pressure) for February 12, 2004, the day of interest used in the analysis.**

3. Results

3.1. Temperature trends across fractions and feature importance

Figure 4 shows the canyon averaged air temperatures (T_{can}) for 9814 simulations (grey lines), along with the T_{can} mean values of clusters of surface fractions, building and vegetation heights (coloured lines). Surface fraction clusters represent the upper value across a 10% range (i.e. 20% includes the range 10 to 20%), and height clusters represent the upper value of an 0.8m range of domain averaged building or tree heights. Note the range of domain averaged heights (0.8 to 4.8 m) differs from the range of individually modelled building or tree heights (0 to 50 m).

In the early morning of February 12th, corresponding to a forcing temperature of approximately 15°C and low wind speeds (less than 2 m/s), the air temperatures for all scenarios (grey lines) show little variation (less than 1°C differences). After 6am, differences quickly develop between the coolest and warmest scenarios, of approximately 5°C at 7am growing to 15-20°C differences by noon and through the afternoon. Corresponding forcing temperatures reach 26°C and wind speeds build to between 5 and 6 m/s. The scenario temperature differences narrow to 5°C by 4pm and in the evening vary by 2-3°C. Forcing temperatures are warmer in this night-time period, dropping from 20 to 17°C with 4 m/s wind speeds.

After dawn, the differences in the clustered mean values begin to increase and reaching a peak at mid-day with maximum differences of approximately 5°C with grass, tree, building fractions and building and vegetation heights. Differences at mid-day reach maximum divergences of 10 and 15°C as street surface fractions reach 80 and 90% respectively. Building and street fractions and building heights drive temperature increases while other types drive reductions.

Figure 5 is similar to Figure 4 but uses ground level calculated means of $UTCI$ from each scenario to calculate the cluster mean values. These timeseries show differences in $UTCI$ (under the same forcing conditions as above) of about 4-5°C in the early morning of February 12th, quickly diverging to 10°C for the majority of the scenarios and closer to 20°C for the scenarios with high percentages of street fractions. In the late afternoon, the range narrows to 10°C and remains at approximately this level through the evening and night.

For surface fraction and height clusters, the night-time ranges of $UTCI$ show wider differences. Increasing building heights, building fractions, and street fractions drive temperature increases both day and night while other types drive reductions. All fractions and heights show a difference of 3°C and greater between the lowest and highest amounts of fractions and heights. These difference remain roughly similar through dawn and until about 8am. Street fractions are the exception and show even wider divergences (5°C and more) starting at 6am. After 6am, differences widen to 5°C for building fractions and building heights and 10°C for tree and grass fractions and vegetation heights. Meanwhile, differences for street fractions grow to nearly 15°C for 80% and over 20°C for 90%.

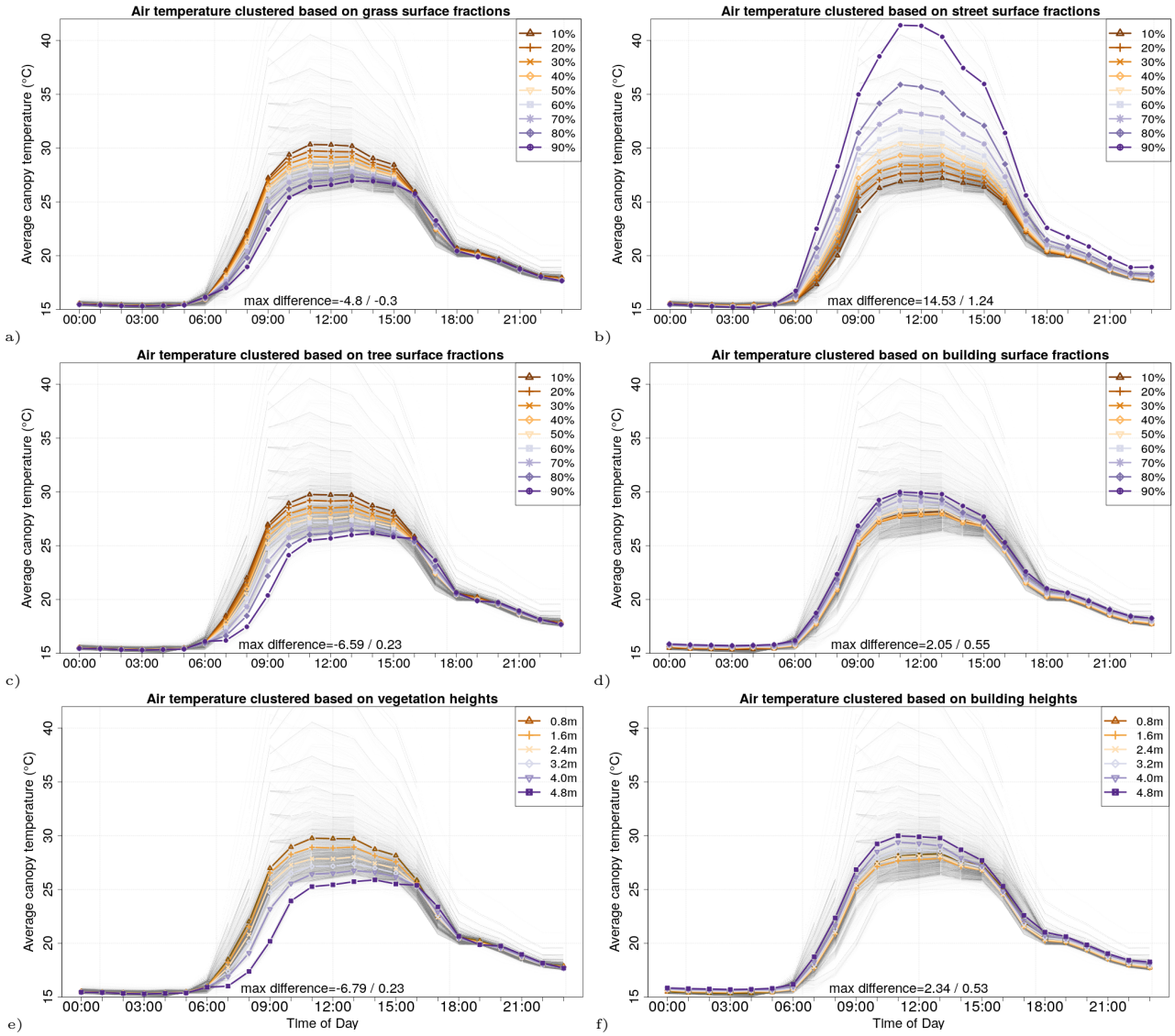

Figure 4: **Canyon averaged air temperature (T_{can}) mean values calculated within clusters of 10% surface fraction ranges of a) grass, b) streets, c) trees, and d) buildings and e) average vegetation and f) average building heights clustered by 0.8m increases for each hour across the diurnal cycle of February 12, 2004. The clusters contain fractions up to the fractional or height breakpoint (i.e. 20% includes the range 10 to 20% while 1.6m includes 0.8 to 1.6m). Annotated maximum difference values for each panel shows the maximum difference between 90% and 10% fractions or 4.8m and 0.8m heights for daytime(6am-10pm)/night-time (10pm-6am). Background grey line plots show temperature timeseries results for all 9814 scenarios for same day.**

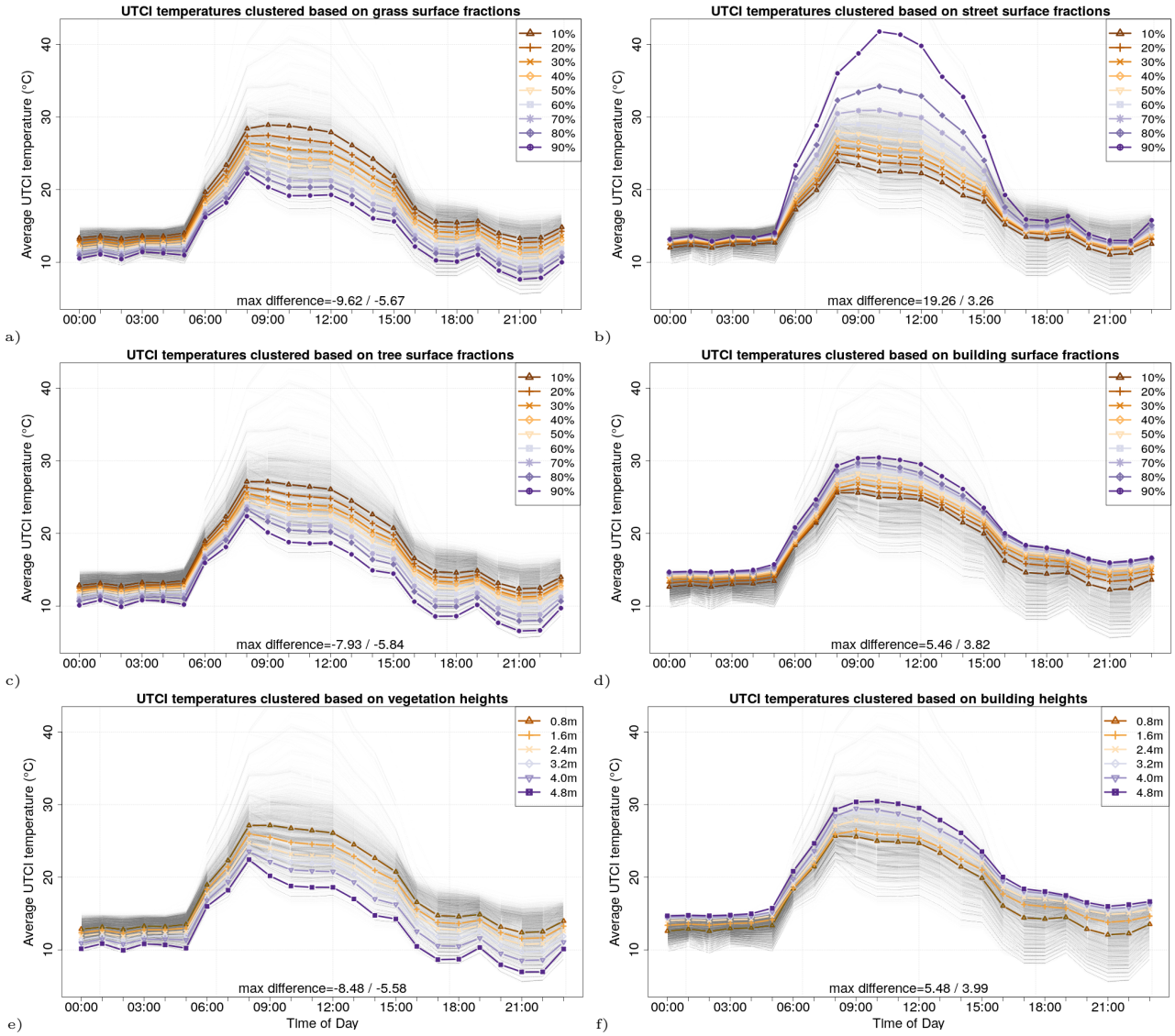

Figure 5: **Means of each scenario's ground level means of $UTCI$, calculated within clusters of 10% surface fraction ranges of a) grass, b) streets, c) trees, and d) buildings and e) average vegetation and f) average building heights clustered by 0.8m increases for each hour across the diurnal cycle of February 12, 2004. The clusters contain fractions up to the fractional or height breakpoint (i.e. 20% includes the range 10 to 20% while 1.6m includes 0.8 to 1.6m). Annotated maximum difference values for each panel shows the maximum difference between 90% and 10% fractions or 4.8m and 0.8m heights for daytime(6am-10pm)/night-time (10pm-6am). Background grey line plots show temperature timeseries results for all 9814 scenarios for same day.**

Table 1: Maximum differences (°C) in T_{can} and $UTCI$ when increasing fractions from 10% to 90% and average vegetation and building heights to 4.4m. Bold indicates temperatures increase as fractions or heights increase. From maximum difference annotations in Figures 4 and 5

Temperature	Time	↑ Trees	↑ Grass	↑ Bld	↑ Street	↑ Veg Ht	↑ Bld Ht
T_{can}	Night	**0.2**	-0.3	**0.6**	**1.2**	**0.2**	**0.5**
T_{can}	Day	-6.6	-4.8	**2.1**	**14.5**	-6.8	**2.3**
$UTCI$	Night	-5.8	-5.7	**3.8**	**3.3**	-5.6	**4.0**
$UTCI$	Day	-7.9	-9.6	**5.5**	**19.3**	-8.5	**5.5**

Figure 6 highlights the range clustered results for two representative warm (2pm) and cool (5am) periods. Upper panels (a, b) show canyon averaged air temperature T_{can}, lower panels (c, d) show ground level $UTCI$ as boxplots for the 9814 scenarios. Note, the number of possible surface type combinations decreases as a single surface type approaches 100%. For example, 90% grass leaves only a small number of combinations for the remaining 10% surface cover. Rankings of feature importance (the influence each features has on predicting a target variable) were calculated for each temperature type (T_{can} and $UTCI$) for the four surface fraction parameters (grass, trees, buildings, and roads) and average vegetation and building heights at each hour during the simulations. The backgrounds of each plot were tinted darker green where a parameter scored higher in feature importance (also see Figure 7).

At 5am, there is a narrow range of T_{can}, from approximately 15.3-16.3°C. Increasing fractions of trees has a slight warming impact with an increase of approximately 0.2°C when increasing trees from 0 to 100%. Increasing vegetation and building heights have almost identical effects. Increasing building and street fractions has a mostly neutral effect but the increasing street fractions start to have a very slight warming impact (0.3°C). Increasing grass fractions has a slight cooling impact of about 0.3°C.

At 2pm, at the warmest time of the day, increasing tree and building fractions and increasing vegetation height continue to provide T_{can} temperature reductions of 1-2°C. Grass fractions and building heights increases show an initial reduction towards the middle fraction ranges then an increase at the higher ranges, with a reduction in the middle ranges of approximately 1°C. Increases in street fractions however show a rapid increase in T_{can} temperatures of approximately 3°C as street fractions approach 80% and another 3°C at 90%.

At 2pm, trends of $UTCI$ amplify the trends seen with T_{can}. Increases in street fractions show increases of approximately 6°C as street fractions approach 80% and another 6°C at 90%. Increasing grass and building heights shows increases of 5°C as fractions or heights increase. Increasing tree and building fractions and tree heights show reductions in temperatures of approximately 5°C.

At 5am, trends of $UTCI$, which include the influences of T_{sfc} and T_{mrt}, show decreases of approximately 2.5°C as fractions of trees and buildings and vegetation heights increase. $UTCI$ increases approximately 3.0°C as grass fractions and building heights increase and 1.5°C as street fractions increase.

Highlighted results are summarised in Table 1, taken from maximum difference annotations in Figures 4 and 5. Analysis of feature importance shows that building fractions and building heights are most significant for T_{can} (Figure 7a) at night while building fractions and building heights are slightly more important than grass and streets and trees and vegetation heights are of the lowest importance for $UTCI$ (Figure 7b). During the daytime, street fractions are of the highest importance for both T_{can} and $UTCI$.

3.2. Distributions of temperatures across a diurnal cycle

The preceding results (Section 3.1) describe domain averaged ground level $UTCI$, however each domain may contain a wide range of $UTCI$ values depending on micro-climate conditions. Therefore Figure 8 shows the intra-domain $UTCI$ distributions for select scenarios for each hour of February 12, 2004.

Figure 8a presents a scenario with very low fractions of roads and buildings and as a result shows $UTCI$ temperatures mostly clustered in the lower ranges across day and night and very few locations that exceed the mid 20s during the day. Figure 8b shows a scenario with a moderate amount of streets and buildings (20% and 30%) and moderate building heights, but yields similar results to Figure 8a. Figure 8d, with higher amounts of buildings and roads, shows a strong shift towards predominately hotter $UTCI$ temperatures (30°C) across the entire domain during the daytime (also reflected in the median), while Figure 8c, with slightly higher fractions of vegetation, shows a similar distribution but the median is much lower (in the lower 20s°C).

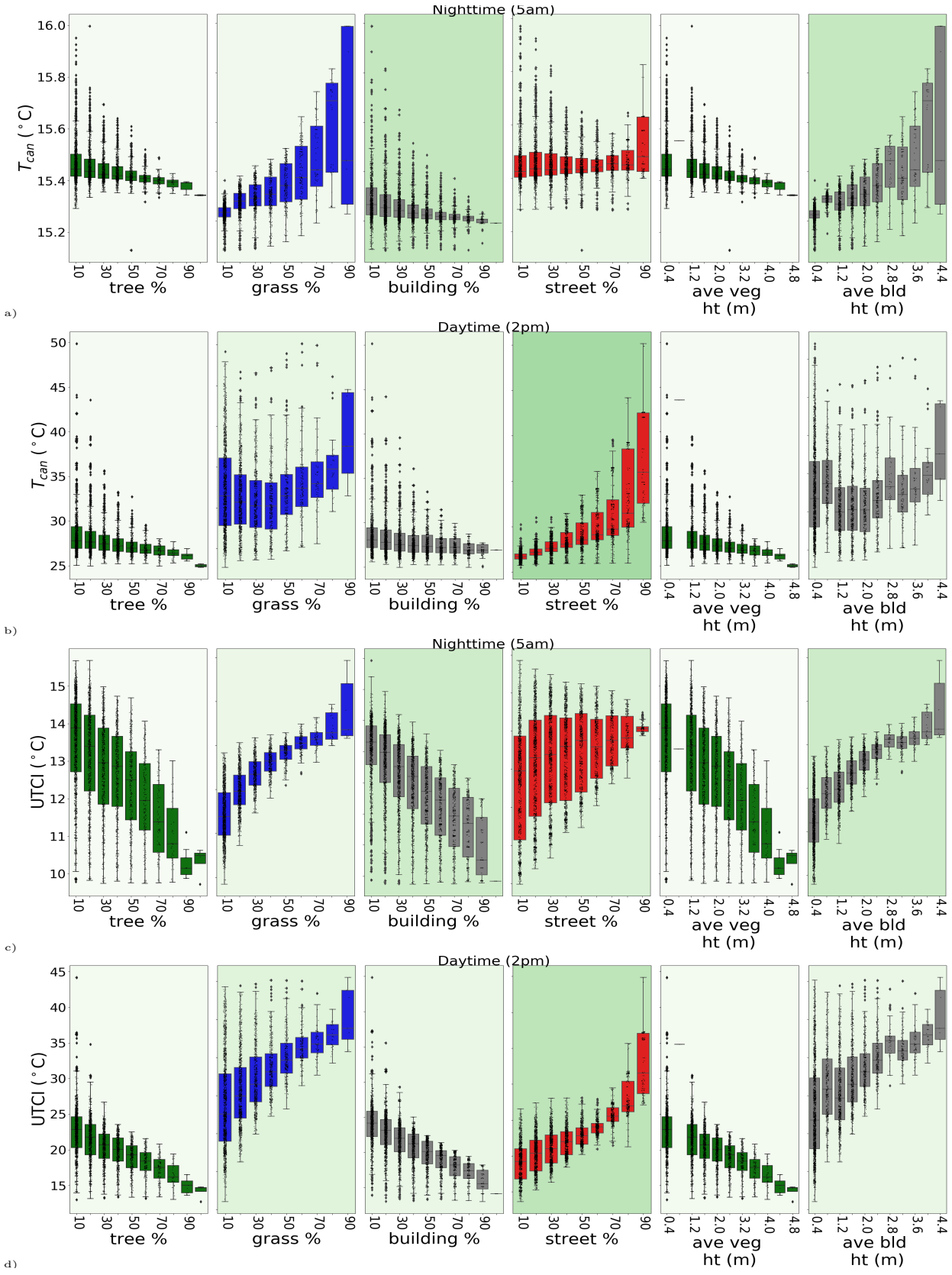

Figure 6: **Surface fraction (trees, grass, buildings, and streets) and average height (vegetation and building) clusters for 9814 scenario's T_{can} and $UTCI$ for February 12, 2004, 5am and 2pm. T_{can} is a single canyon averaged air temperature while $UTCI$ is a calculated mean at ground level. The clusters will contain fractions up to the fractional or height breakpoint (i.e. 20% includes the range 10 to 20% while 1.6m includes 1.2 to 1.6m). Feature importance for each temperature type is indicated by the green background tinting.**

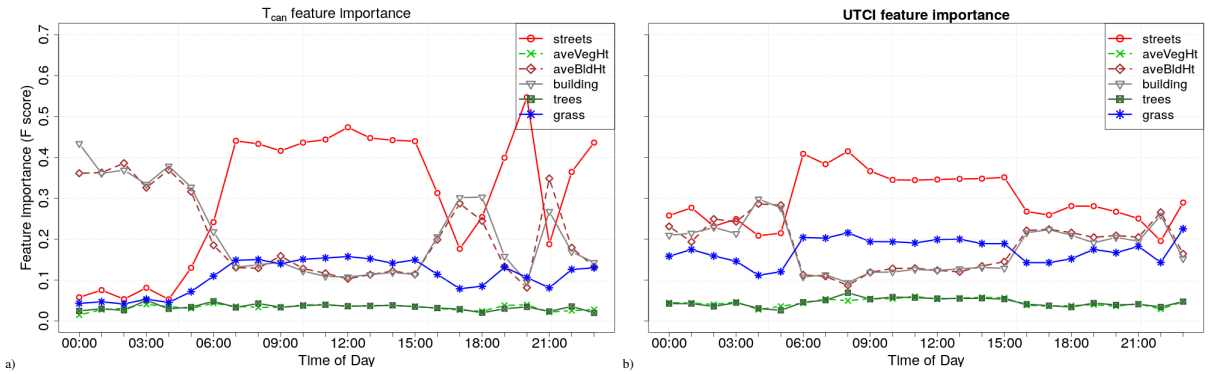

Figure 7: **Feature importance in a)** T_{can} **and b)** $UTCI$ **for the four surface fractions of streets, buildings, trees, and grass and average heights of vegetation and buildings across February 12, 2004.**

These four example distributions show that urban heat has high variability at a micro-scale, even between scenarios with similar urban form and surface fractions. Mean temperature values (such as Table 1) can show general trends but each of these four distributions will contribute to four very different spatial experiences of urban heat and human thermal stress in each domain.

4. Discussion

4.1. The influence of urban surfaces on urban heat

Studies providing a systematic examination of the influence of varying surface fractions and urban heights are rare and generally based on remote sensing data. In this study, through systematic micro-climate modelling of a comprehensive range of surface fractions and average heights, the importance and relative influence of each feature type on the temperature types of T_{can} and $UTCI$ was examined. For T_{can}, at night-time, a narrow range of temperature variations were found, of approximately 1.0°C. Wind speed on February 12th (Figure 3) was approximately 2m/s until the early afternoon, rising to approximately 6m/s, then dropping to 4 m/s after sunset. These higher wind speeds in the afternoon and evening had the effect of reducing the range of temperature variations in the evening and night compared to Stewart et al. (2021) where forcing wind speed was set to a constant 2.5m/s and resulted in wider ranges of night-time temperatures.

In the presence of high wind speed at night, increasing fractions of trees had a limited impact at midnight and contributed to a very slight increase (+0.2°C) at dawn. Increasing building heights had a warming impact (+1.2°C) while grass drove a slight cooling (-0.3°C). Increasing street fractions contributed to a warming effect (+0.3°C) at dawn. Building fractions and building heights were found to be the most significant features at night-time. During the daytime, the most important feature was the fraction of streets. Street fractions of 80 and 90% can drive T_{can} increases of up to 10 and 15°C respectively while reductions are seen of about -5°C when increasing grass and tree fractions from 0 to 100%.

Some ground level LCZ based studies can provide some comparisons with our results. Holmer et al. (2013) finds that large vegetated sites cool quickly (have a large cooling rate) for 1-2 hours after sunset then cooling rates reduce and align with those of sparely vegetated sites for the rest of the night. We find that in air temperature, areas with high building heights and building fractions cools rapidly after sunset where in terms of $UTCI$, areas with large trees and tree fractions cool most rapidly. In air temperatures differences observed across a year, Yang et al. (2018) finds LCZD (irrigated agriculture) is the coolest class in Nanjing, China while variations of LCZ2 (compact mid-rise but with different amounts of tree cover) are 2-3°C warmer (those in the lower range have higher amounts of trees), LCZ4 (open high-rise) and LCZ8 (large low-rise) are 1.6 and 1.8°C warmer respectively, and LCZ10 (heavy industry) is 2.7°C warmer. These are generally in line with our findings. LCZ10 is mostly low rise and highly imperious and similar to our high street fraction scenarios which were substantially hotter than most other urban arrangements. Increasing fractions of trees had a moderating effect across all the scenarios. Finally, Puliafito et al. (2013) in comparing average air temperatures and Physiologically Equivalent Temperatures (PET) across transits of different LCZs to the mean of

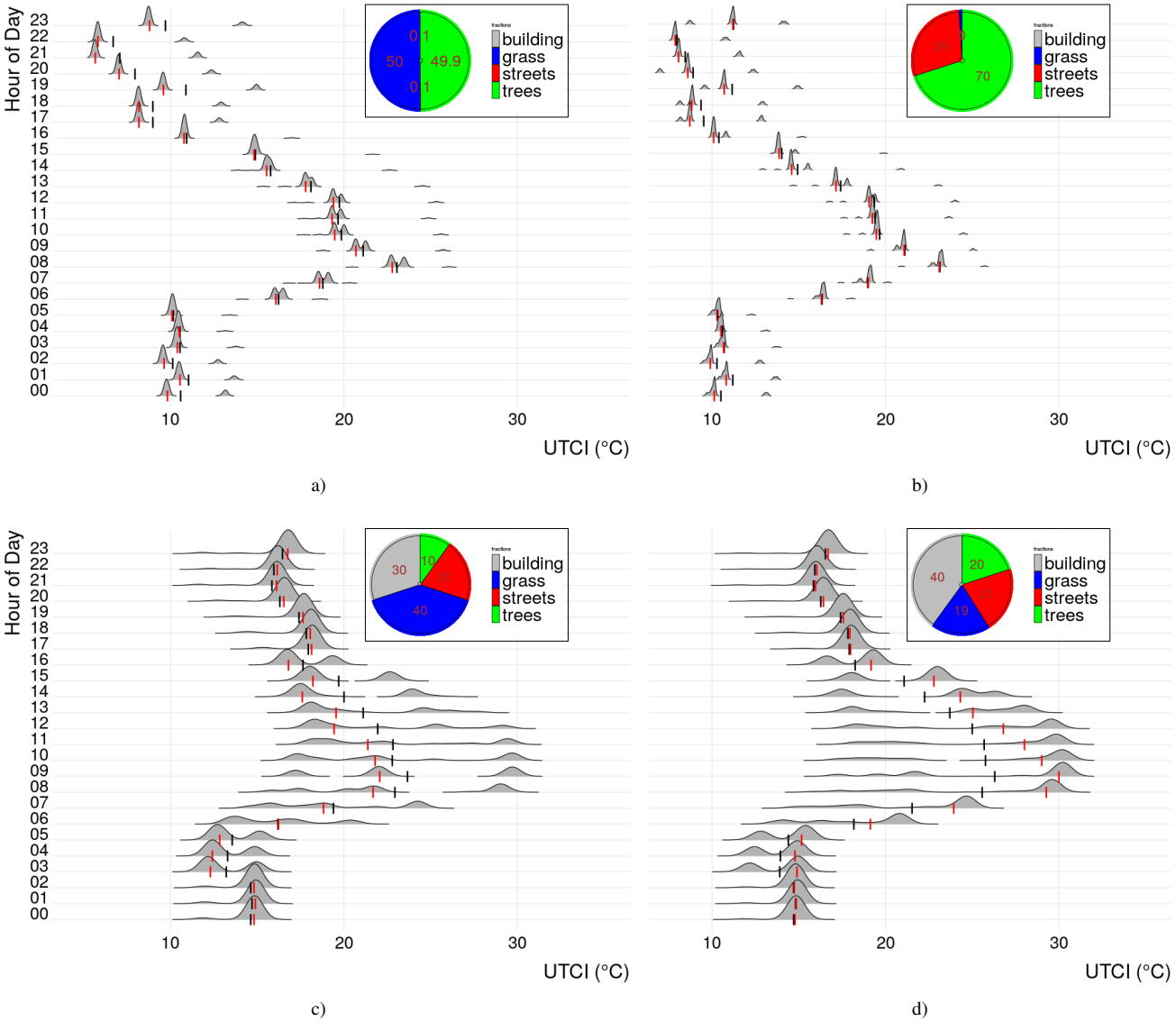

Figure 8: **Distribution of *UTCI* across February 12, 2004 for scenarios a) 50% grass, 49.99% trees, 0.01% road, 0% building, average vegetation height of 4m, and average building height of 0m, b) 29% grass, 69% trees, 1% road, 1% building, average vegetation height of 0.5m, and average building height of 5m, c) 40% grass, 10% trees, 20% road, 30% building, average vegetation height of 2m, and average building height of 14m, and d) 19% grass, 20% trees, 21% road, 40% building, average vegetation height of 1m, and average building height of 9m. Insert shows percent fractions of surface types. Hourly medians are annotated in red and hourly means in black.**

all their observations find the largest air temperature reductions of approximately 2°C in the mornings and evenings in LCZD (0.6°C in the afternoon), up to 1°C reductions in the evening for LCZ3A (residential/dense trees) and LCZA (parks). Increases in air temperatures are observed of 1.5, 1.1, and 0°C in downtown areas with scattered trees, medium trees, and high trees respectively. Trends in thermal comfort, PET, are similar but with larger magnitudes (i.e. -3.5°C in LCZA), but at mid-day in the three downtown areas with varying tree cover the respective differences are 3.4, -0.2, and -5.3°C PET. Vegetated areas have the largest air temperature reductions with the amount of tree cover a major factor in the magnitudes, while the differing thermal comfort benefits were strongly driven by amounts and heights of trees, but only at mid-day.

Other studies show similar findings, often they were only able to demonstrate temperature trends rather than more detailed relationships. Emery et al. (2021), in their observations of the influence of different LCZ classes on air temperature, found that the LCZ classes with the warmest air temperatures were those dominated by artificial, mineral, and impervious surfaces, while LCZ classes with vegetation were the coolest. However, they were not able to quantify the ranges of temperatures in more detail resulting from the different classes. Using remotely sensed LST, Alexander (2021) classified areas in a number of Danish cities into two classes of buildings and vegetation (essentially impervious vs. pervious) and into ranges of vegetation and building heights and examined their influence on LST. He found LST reduced by approximately 4°C when vegetation fractions increased from 0-5 to 95-100% and increased by 4°C when building fractions increased by the same. Also, vegetation height had negative correlation with LST but vegetation cover was found to be a stronger predictor. Building height had a positive correlation with LST, but only up to 9m, and was not always found to have a strong influence on LST in some of the studied cities.

Peng et al. (2022) found, using a Random Forest regression of MODIS LST observations of a highly urbanised city in Japan, the feature importance to predict urban heat island intensity in the daytime was highest for building density followed by distance to green space while at night-time distance to green space was the most important followed by distance to water and road density. In another study, using Landsat derived LST of different LCZ classes across four African cities (Li et al., 2022), the highest LST temperatures were found in the urban typologies of compact mid-rise, compact low-rise, and large low-rise (LCZ2, 3, and 8) and lowest in dense trees and water (LCZA and G). They found statistically significant differences between the LCZs, but not always when comparing LCZ classes in different cities of different Köppen climate classifications, where often compact midrise (LCZ2) and open midrise (LCZ5) typologies were coolest (due to higher building heights). The LCZ typologies were found to be useful across single cities but could not always reliably be used to compare LCZ classes across different cities, especially those with differing climates.

While these results are able to show broad trends due to differing amounts of surface fractions, linking LST temperatures to thermal comfort at ground level can be challenging and potentially misleading (Coutts et al., 2016; Stewart et al., 2021) as surface temperatures underneath the urban canopy are moderated by shading from vegetation and buildings (Coutts et al., 2015; Lee et al., 2018; Krayenhoff et al., 2021). This is a limitation of remotely sensed LST observations, that can only provide the temperatures at the top of the urban canopy. Some studies are able to provide some additional data on the under canopy impacts through observations. For example, micro-climate observations from Broadbent et al. (2017) showed that in a residential suburb, T_{sfc} temperatures of concrete, buildings, and bare ground were 2.4, 3.1, and 1.1°C hotter than the area averages during the day and areas with trees, irrigated grass, and low vegetation were 3.0, 7.7, and 6.8°C cooler. While high resolution spatial air temperature are difficult to observe, Broadbent et al. (2017) also found increases over the suburb average in air temperature of 1°C in the cluster type of urban mid-rise and 0.5°C with the type urban residential. They also found an irrigated grass daytime cooling effect of -0.1°C per 5% fraction increase. Middel and Krayenhoff (2019) found trees could provide large reductions in T_{mrt} on extreme heat days, with reductions up to 33.4°C and with sky view factor (SVF) highly influential in determining the reductions, 4°C T_{mrt} reductions per 0.1 SVF decreases. However, the trade-offs are a warming effect at night of up to 5°C. In addition, they found replacing impervious with pervious surfaces can decrease T_{mrt} by 1.0-1.5°C per tenth of land converted and unshaded irrigated grass could reduce T_{mrt} by more than 10°C compared to impervious surfaces with unirrigated grass providing still about half as much in reductions. Additionally, Krayenhoff et al. (2021) finds that trees provide additional 0.3°C reductions per 0.10 canopy cover increase.

The results reported in the studies compared above of trends and relationships between different urban forms and observed temperature outcomes (both air temperatures and thermal comfort indexes) demonstrates the difficulty in designing and testing mitigation measures that are based on changing individual design parameters once at time. Quantifying the impact of the measures, when in reality each urban change is interdependent on other elements

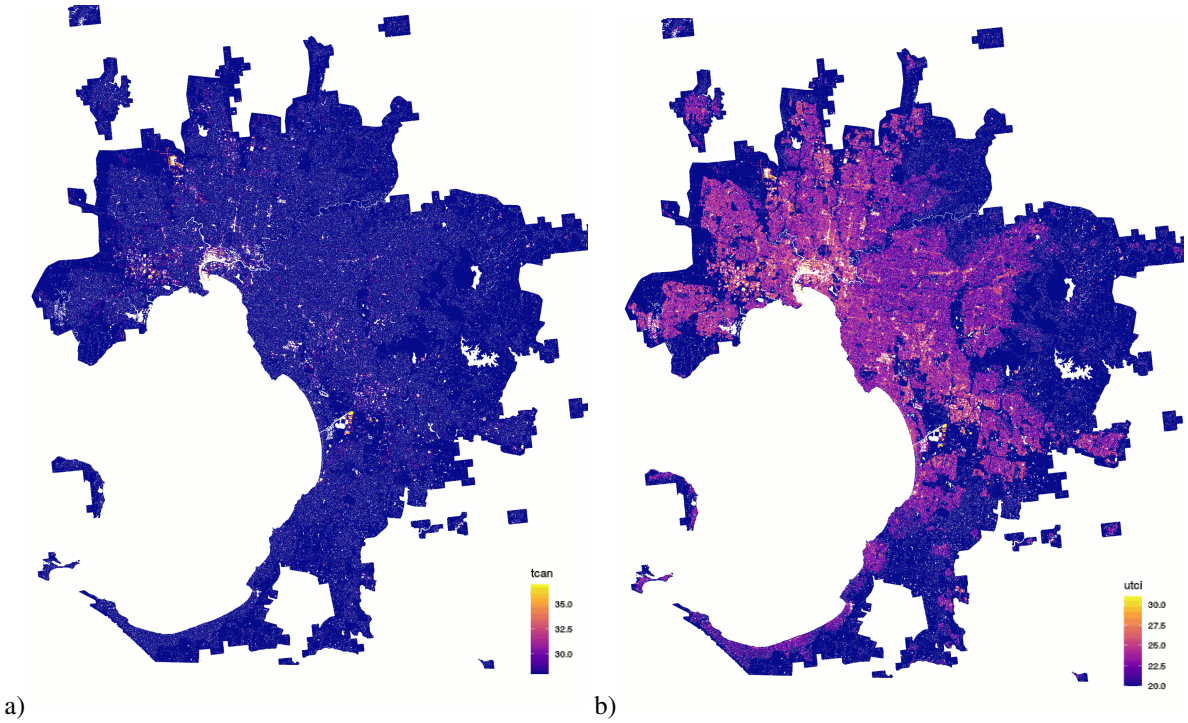

Figure 9: **a)** T_{can} **and b)** $UTCI$ **heatmaps on February 12, 2004 at 2pm generated by matching the closest matching parameters of surface fractions and average heights for each 100×100m location in Melbourne from 9814 modelled scenario results (in** °C**).**

of urban form and moderate the impacts (often in a non-linear fashion), make quantifying their impacts difficult. This is especially true when the additional complexity of regional geography and human activity is added into the mix. This points to the necessity of a modelling approach that can examine a comprehensive range of representative combinations of urban form at once and in isolation from as many other compounding interdependencies to overcome the difficulties in attributing the influence of each individual urban element and allow a generalisation of the findings to other scenarios and cities.

4.2. City scale heat maps from micro-climate modelled results

Following on from the results of the comprehensive urban form analysis and reflecting many of the specific findings of other studies of the impact of differing types of urban form on urban heat, the modelled results underlying this analysis were applied to demonstrate their application to a city-wide heat mapping exercise. These heat maps show the impact of present day urban form across a number of Australian cities, isolated from geography, topography, and local weather conditions. Surface fractions and average building and vegetation heights for Melbourne and Sydney were calculated for 100×100m locations using 2 meter resolution land cover and building and tree footprints and heights from Geoscape (Geoscape, 2020). Figure 9 shows city-wide heat maps of T_{can} and $UTCI$ in Melbourne at 2pm on February 12, 2004 constructed by matching the closest matching parameters for each locations from the 9814 modelled scenario results. A narrow range of air temperatures are seen across most of the city, closely aligned to the modelling forcing temperature at 2pm of 25.9°C. Higher temperatures can be seen in areas corresponding to higher fractions of roads and to a lesser degree of buildings. No particular reductions of air temperatures are seen in areas corresponding to higher levels of trees or grass surface fractions. Fractional breakdowns of surfaces types across Melbourne are shown in Supplementary Figure S1.

Wider ranges of surface temperatures are seen across Melbourne. Some slight reductions of surface temperatures (below the forcing air temperature) are seen in areas that correspond to higher fractions of grass and of trees. However, strong increases in surface temperatures are seen in areas with higher fractions of street surfaces, even in areas with street fractions as low as 30%. Very strong increases in surface temperatures can be seen in areas with high street

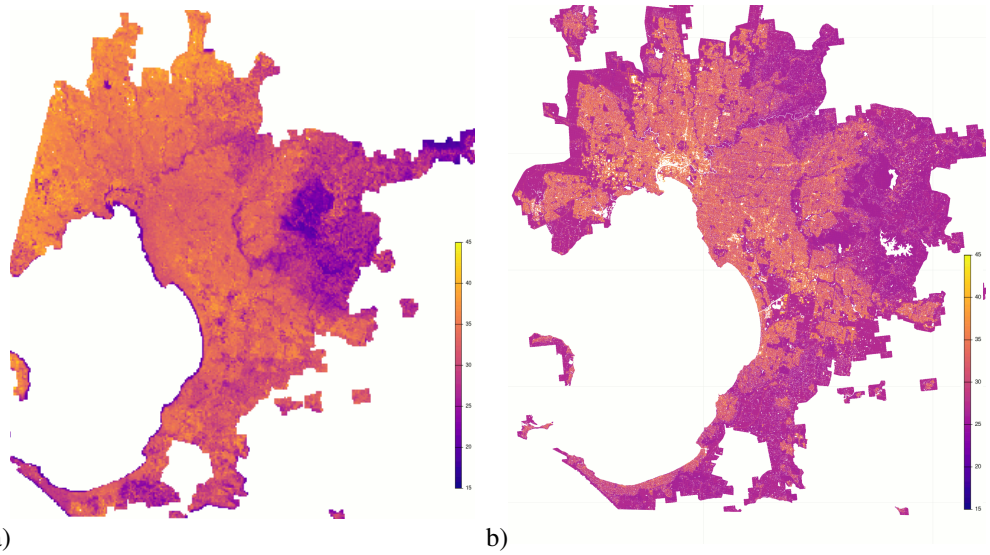

a) b)

Figure 10: **a) Landsat 8 land surface temperature (°C) captured 10am December 11, 2018. Local conditions of air temperature on this day were minimum and maximum of 22 and 26°C. b) Modelled T_{sfc} (°C) on February 12, 2004 at 10am generated by matching the closest matching parameters of surface fractions and average heights for each 100×100m location in Melbourne from 9814 modelled scenario results.**

surface fractions, for example Melbourne Airport in the north west, the central business district (CBD) in the city centre, and Moorabbin Airport in the city south east.

Figure 10 presents a comparison of modelled T_{sfc} to Landsat 8 LST data. Figure 10a shows Landsat 8 imagery captured on a cloudless day that mostly closely corresponds to the modelled conditions, 10am December 11, 2018 when local conditions of air temperature on this day were minimum and maximum of 22 and 26°C. Figure 10b shows T_{sfc} created from modelled results at 10am on February 12, 2004 and February 14, 2004.

In comparing the constructed T_{sfc} heat maps with the LST imagery, some observations can be made. However note, the two datasets measure different things and might not be entirely comparable. LST observations are captured by satellite and correspond to temperatures at the top of the urban canopy (i.e. the tops of trees and buildings) while the modelled T_{sfc} corresponds to ground surface temperatures and will generally be cooler as they include areas that are shaded by tree canopies and buildings. In addition, LST observations are influenced by additional factors than just the urban form including topography and localised weather conditions. In Figure 10a, the cooler locations in the LST observations mostly include locations immediately off the coast and in the eastern fringes of Melbourne, the Dandenong Ranges which range from 500m to over 1000m in elevation, while the majority of central and inner Melbourne is under 100m in elevation. The main differences between the LST observations and the modelled results are strongly related to the surface fraction types, which a strong correlation between the differences and building and street fractions and a strong negative correlation with grass surface fractions.

Additionally, heat maps were generated for other cities. Using the 9814 modelled scenario results, heat maps of T_{can} and $UTCI$ (Supplementary Figure S3) were created for Sydney for February 12, 2004 at 2pm by matching the closest matching parameters, as calculated from Supplementary Figure S2, for each location. Supplementary Figure S4a shows cloudless Landsat 8 observations from 10am March 11, 2019 (local conditions of air temperature on this day were minimum and maximum of 22 and 26°C) while Supplementary Figure S3b shows T_{sfc} heatmaps created from modelled results at 10am on February 12, 2004.

The results are similar to those from Melbourne. Ranges of T_{can} are generally very narrow with small localised hot spots. The LST observations reflect a different topography than Melbourne with a larger influence of coastal features and a smaller range of elevations. Much of the central city is under 100m elevation and only approaching 200m in the north east areas. The areas with higher ranges of LST are concentrated in the western regions of the city (with very high percentages of grass/low vegetation land cover fractions). Similar to Melbourne, LST and T_{sfc} are strongly negatively correlated with grass fractions but somewhat less correlated with building and street fractions.

This study demonstrates a new method of massive ensemble modelling, to efficiently perform city scale modelling at a micro-scale to isolate the impacts of the urban form and fabric on urban heat. The overall method can be replicated with any suitable micro-climate scaled model (or with improved versions of VTUF-3D). Future work has been planned to address two potential limitations of this study: model bias and expanding the range of representative weather conditions. VTUF-3D has been extensively evaluated using the forcing data used in this study, but like all models, has biases. VTUF-3D might underestimate surface temperatures of grass. Analysis of correlations between the surface fractions and differences between observed LST and modelled T_{sfc} suggest that the temperature trends for streets (correlations of 0.69 and 0.72 in Melbourne respectively) and buildings (0.78 and 0.72 in Melbourne) are reasonable but the magnitude is too high while grass (-0.80 and -0.85) trends are also reasonable but too low. Meanwhile the correlations for trees are very low suggesting the variations are not regular. As the percent fractions for trees just means that tree cover exists, it does not fully characterise the tree cover, such as the level of canopy cover (i.e. a leaf area index) or the variations in coverage amounts. VTUF-3D is undergoing continuous improvement, especially its vegetation scheme, and future research will apply these improvements to similar assessments. A second limitation planned to be addressed with further research is to ensure the method models a full set of representative days and weather types for a city. For this, weather clustering (Shobha and Asha, 2017; Acero et al., 2019; Nazarian et al., 2019) will be utilised to generate forcing data for the full range of weather condition types experienced in cities and allow the analysis of thermal comfort across the range of extreme heat days to warm down to extreme cold winter days.

5. Conclusion

Observational studies have previously attempted to quantify the influence of urban form on urban heat largely using two different types of observations, remotely sensed LST and under the urban canopy ground level micro-scaled observations. Satellite or aerial remote sensing observes only sky-facing surfaces (e.g. roofs and the vegetation canopy). Micro-scaled ground based observations can provide detailed assessments under the canopy, but are time-intensive, requiring substantial effort to collect, and are difficult to scale up to a city-wide scale. The observations reported in these studies show many of the trends found in this study, including the large increases in both T_{can} and $UTCI$ with increasing road fractions, as well as decreases of both temperature types during the daytime with increasing vegetation fractions and heights. Our method also overcomes difficulties encountered with the LCZ-based observations and modelling assessments, where the highly urbanised classes were found to be hotter while the natural classes were cooler, findings in line with our results. However, due to the broad range of possible morphology within each LCZ along with the (often non-linear) interactions between the parameters, detailed quantification has not always been possible in the studies utilising LCZs (i.e. Emery et al. (2021)).

Using the comprehensive urban form analysis methods in this study allows a determination of the importance and relative influence of each surface type and feature height on thermal performance (e.g. increasing street fractions from 50% to 80% can drive air temperature increases of up to 5°C). Additionally, once these relationships have been quantified, it becomes possible to apply the results across a broad area, a city-wide assessment of thermal comfort. This is an area of broad interest as evidenced by the numerous studies attempting this through satellite observed LST. However, a comprehensive modelling approach is able to capture both sky-facing and pedestrian-level conditions at city scales. Additionally, it removes geographic influences (such as topography, ocean effects, and local weather) from the results and allows an assessment based solely on the urban and natural forms of the urban areas. This allows an assessment at city scales of problematic existing urban form, and allows mitigation strategies to be tested based on the urban form elements that can be changed, while removed from influences that cannot be redesigned. Heat can often be inequitably distributed (Jenerette, 2018; Nazarian et al., 2021; Guardaro et al., 2022) where more challenging thermal conditions can be experienced in parts of urban areas with low levels of vegetation and canopy cover and high impervious surface fractions compared to leafy enclaves near large water bodies. Understanding the impacts of the urban form can help weigh the relative importance of urban interventions, providing local context to the anticipated impact of the intervention with the required urgency.

6. References

Acero, J. A., Koh, E. J. K., Pignatta, G., Norford, L. K., 2019. Clustering weather types for urban outdoor thermal comfort evaluation in a tropical area. Theor. Appl. Climatol.

Alexander, C., 2021. Influence of the proportion, height and proximity of vegetation and buildings on urban land surface temperature. International Journal of Applied Earth Observations and Geoinformation 95, 102265.
URL https://doi.org/10.1016/j.jag.2020.102265

Best, M. J., Grimmond, C. S. B., 2012. Analysis of the Seasonal Cycle Within the First International Urban Land-Surface Model Comparison. Boundary-Layer Meteorology 146 (3), 421–446.

Bowler, D. E., Buyung-Ali, L., Knight, T. M., Pullin, A. S., 2010. Urban greening to cool towns and cities: A systematic review of the empirical evidence. Landscape and Urban Planning 97 (3), 147–155.

Broadbent, A. M., Coutts, A. M., Tapper, N. J., Demuzere, M., Beringer, J., 2017. The microscale cooling effects of water sensitive urban design and irrigation in a suburban environment. Theor. Appl. Climatol., 1–23.

Bröde, P., Fiala, D., Blazejczyk, K., Holmér, I., Jendritzky, G., Kampmann, B., Tinz, B., Havenith, G., 2012. Deriving the operational procedure for the Universal Thermal Climate Index (UTCI). International Journal of Biometeorology 56 (3), 481–494.

Bruse, M., 1999. The influences of local environmental design on microclimate- development of a prognostic numerical Model ENVI-met for the simulation of Wind, temperature and humidity distribution in urban structures. Ph.D. thesis, University of Bochum, Germany (in German).

Bureau of Meteorology, 2021. Long-term temperature record: Australian Climate Observations Reference Network - Surface Air Temperature (ACORN-SAT).
URL http://www.bom.gov.au/climate/data/acorn-sat/

Cheung, P. K., Livesley, S. J., Nice, K. A., 2021. Estimating the cooling potential of irrigating green spaces in 100 global cities with arid, temperate or continental climates. Sustainable Cities and Society, 102974.
URL https://doi.org/10.1016/j.scs.2021.102974

Ching, J., Aliaga, D., Mills, G., Masson, V., See, L., Neophytou, M., Middel, A., Baklanov, A., Ren, C., Ng, E., Fung, J., Wong, M., Huang, Y., Martilli, A., Brousse, O., Stewart, I., Zhang, X., Shehata, A., Miao, S., Wang, X., Wang, W., Yamagata, Y., Duarte, D., Li, Y., Feddema, J., Bechtel, B., Hidalgo, J., Roustan, Y., Kim, Y., Simon, H., Kropp, T., Bruse, M., Lindberg, F., Grimmond, S., Demuzure, M., Chen, F., Li, C., Gonzales-Cruz, J., Bornstein, B., He, Q., Hanna, A., Erell, E., Tapper, N., Mall, R. K., Niyogi, D., 2019. Pathway using WUDAPT's Digital Synthetic City tool towards generating urban canopy parameters for multi-scale urban atmospheric modeling. Urban Climate 28, 100459.
URL https://www.sciencedirect.com/science/article/abs/pii/S2212095519300975

Coates, L., Haynes, K., O'Brien, J., et al., 2014. Exploring 167 years of vulnerability: An examination of extreme heat events in Australia 1844-2010. Environmental Science and Policy 42, 33–44.
URL http://dx.doi.org/10.1016/j.envsci.2014.05.003 https://www.sciencedirect.com/science/article/pii/S1462901114000999

Coffel, E. D., Horton, R. M., de Sherbinin, A., 2018. Temperature and humidity based projections of a rapid rise in global heat stress exposure during the 21st century. Environ. Res. Lett. 13, 014001.

Coutts, A. M., Beringer, J., Tapper, N. J., 2007. Impact of Increasing Urban Density on Local Climate: Spatial and Temporal Variations in the Surface Energy Balance in Melbourne, Australia. Journal of Applied Meteorology and Climatology 46 (4), 477–493.
URL http://journals.ametsoc.org/doi/abs/10.1175/JAM2462.1

Coutts, A. M., Harris, R. J., Phan, T., Livesley, S. J., Williams, N. S., Tapper, N. J., 2016. Thermal infrared remote sensing of urban heat: Hotspots, vegetation, and an assessment of techniques for use in urban planning. Remote Sensing of Environment 186, 637–651.
URL http://dx.doi.org/10.1016/j.rse.2016.09.007

Coutts, A. M., Tapper, N. J., Beringer, J., Loughnan, M., Demuzere, M., 2012. Watering our Cities: The capacity for Water Sensitive Urban Design to support urban cooling and improve human thermal comfort in the Australian context. Progress in Physical Geography 37 (1), 2–28.
URL http://ppg.sagepub.com/cgi/doi/10.1177/0309133312461032

Coutts, A. M., White, E. C., Tapper, N. J., Beringer, J., Livesley, S. J., 2015. Temperature and human thermal comfort effects of street trees across three contrasting street canyon environments. Theoretical and Applied Climatology 124 (1), 55–68.
URL http://link.springer.com/10.1007/s00704-015-1409-y

Dominik, F., Andreas, M., 2019. Calculating human thermal comfort and thermal stress in the PALM model system 6.0. Geoscientific Model Development Discussions, 1–21.
URL https://www.geosci-model-dev-discuss.net/gmd-2019-202/

Emery, J., Pohl, B., Cretat, J., Richard, Y., Pergaud, J., Rega, M., Zito, S., Dudek, J., Vairet, T., Joly, D., Thevein, T., 2021. How local climate zones influence urban air temperature: Measurements by bicycle in Dijon, France. Urban Climate 40, 101017.

Erell, E., Williamson, T., 2006. Simulating air temperature in an urban street canyon in all weather conditions using measured data at a reference meteorological station. International Journal of Climatology 26 (12), 1671–1694.
URL http://onlinelibrary.wiley.com/doi/10.1002/joc.1328/abstract

Forzieri, G., Cescatti, A., Batista, F., Feyen, L., 2017. Increasing risk over time of weather-related hazards to the European population: a data-driven prognostic study. Lancet Planet Health 1 (5), e200–e208.
URL http://dx.doi.org/10.1016/S2542-5196(17)30082-7

Geoscape, 2020. Australian Spatial data for 3D buildings, building heights & land parcels. https://geoscape.com.au/.

Guardaro, M., Hondula, D. M., Ortiz, J., Redman, C. L., 2022. Adaptive capacity to extreme urban heat: The dynamics of differing narratives. Climate Risk Management 35, 100415.
URL https://doi.org/10.1016/j.crm.2022.100415

Hammerberg, K., Brousse, O., Martilli, A., Mahdavi, A., 2018. Implications of employing detailed urban canopy parameters for mesoscale climate modelling: a comparison between WUDAPT and GIS databases over Vienna, Austria. International Journal of Climatology 38, e1241–e1257.

Hendel, M., Gutierrez, P., Colombert, M., Diab, Y., Royon, L., 2016. Measuring the effects of urban heat island mitigation techniques in the field:

Application to the case of pavement-watering in Paris. Urban Climate 16, 43–58.
URL http://dx.doi.org/10.1016/j.uclim.2016.02.003

Hettrich, S., Maronga, B., Raasch, S., 2020. PALM-4U A building-resolving microscale model to support future adaptation of cities in a changing urban climate. In: EGU General Assembly 2020, Online, 4-8 May 2020.

Holmer, B., Thorsson, S., Linden, J., 2013. Evening evapotranspirative cooling in relation to vegetation and urban geometry in the city of Ouagadougou, Burkina Faso. Int. J. Climatol. 3105, 3089–3105.

IPCC, 2022. Climate Change 2022: Impacts, Adaptation, and Vulnerability. Contribution of Working Group II to the Sixth Assessment Report of the Intergovernmental Panel on Climate Change. Cambridge University Press.

Jacobs, S., Gallant, A., Tapper, N., Li, D., 2018. Use of cool roofs and vegetation to mitigate urban heat and improve human thermal stress in Melbourne, Australia. J. Appl. Meteor. Climatol.
URL https://journals.ametsoc.org/doi/abs/10.1175/JAMC-D-17-0243.1

Jenerette, G. D., 2018. Ecological contributions to human health in cities. Landscape Ecology.
URL http://link.springer.com/10.1007/s10980-018-0708-y

Krayenhoff, E. S., Broadbent, A. M., Zhao, L., Georgescu, M., Middel, A., Voogt, J. A., Martilli, A., Sailor, D. J., Erell, E., 2021. Cooling hot cities: A systematic and critical review of the numerical modelling literature. Environ. Res. Lett.

Lee, I., Voogt, J., Gillespie, T., 2018. Analysis and Comparison of Shading Strategies to Increase Human Thermal Comfort in Urban Areas. Atmosphere 9 (3), 91.
URL http://www.mdpi.com/2073-4433/9/3/91

Li, X., Stringer, L. C., Dallimer, M., 2022. The role of blue green infrastructure in the urban thermal environment across seasons and local climate zones in East Africa. Sustainable Cities and Society 80, 103798.
URL https://doi.org/10.1016/j.scs.2022.103798

Lindberg, F., Grimmond, C. S., Gabey, A., et al., 2018. Urban Multi-scale Environmental Predictor (UMEP): An integrated tool for city-based climate services. Environmental Modelling and Software 99, 70–87.

Martilli, A., Krayenhoff, E. S., Nazarian, N., 2020. Is the Urban Heat Island intensity relevant for heat mitigation studies? Urban Climate 31.
URL https://www.sciencedirect.com/science/article/pii/S2212095519300070

Masson, V., 2005. Urban surface modeling and the meso-scale impact of cities. Theoretical and Applied Climatology 84 (1-3), 35–45.
URL http://www.springerlink.com/index/10.1007/s00704-005-0142-3

Masson, V., Heldens, W., Bocher, E., Bonhomme, M., Bucher, B., Burmeister, C., Munck, C. D., Esch, T., Hidalgo, J., Kanani-Sühring, F., Kwok, Y.-T., Lemonsu, A., Lévy, J.-P., Maronga, B., Pavlik, D., Petit, G., See, L., Schoetter, R., Tornay, N., Votsis, A., Zeidler, J., 2020a. City-descriptive input data for urban climate models: Model requirements, data sources and challenges. Urban Climate 31, 100536.
URL https://doi.org/10.1016/j.uclim.2019.100536

Masson, V., Lemonsu, A., Hidalgo, J., Voogt, J., 2020b. Urban Climates and Climate Change. Annu. Rev. Environ. Resour., 411–444.

Middel, A., Krayenhoff, E. S., 2019. Micrometeorological determinants of pedestrian thermal exposure during record-breaking heat in Tempe, Arizona: Introducing the MaRTy observational platform. Science of the Total Environment 687, 137–151.
URL https://doi.org/10.1016/j.scitotenv.2019.06.085

Middel, A., Turner, V. K., Schneider, F. A., Zhang, Y., Stiller, M., 2020. Solar reflective pavements A policy panacea to heat mitigation? Environ. Res. Lett.

Mills, G., Ching, J., Bechtel, B., 2021. Characterising urban morphology for urban climate modelling. In: Urban Climate Science for Planning Healthy Cities. Springer, pp. 339–354.

Milošević, D. D., Savić, S. M., Marković, V., Arsenović, D., Šećerov, I., 2016. Outdoor human thermal comfort in local climate zones of Novi Sad (Serbia) during heat wave period. Hungarian Geographical Bulletin 65 (2), 129–137.

Nazarian, N., Acero, J. A., Norford, L., 2019. Outdoor thermal comfort autonomy: Performance metrics for climate-conscious urban design. Building and environment 155, 145–160.

Nazarian, N., Fan, J., Sin, T., Norford, L., Kleissl, J., 2017. Predicting outdoor thermal comfort in urban environments: A 3d numerical model for standard effective temperature. Urban Climate 20, 251–267.
URL https://www.sciencedirect.com/science/article/pii/S2212095517300354

Nazarian, N., Krayenhoff, E. S., Bechtel, B., Hondula, D., Paolini, R., Vanos, J., Cheung, T., Chow, W. T. L., de Dear, R., Jay, O., Lee, J. K. W., Martilli, A., Middel, A., Norford, L. K., Sadeghi, M., Santamouris, M., Schiavon, S., 2021. Integrated Assessment of Urban Overheating Impacts on Human Life. ESSOAr.

Nazarian, N., Sin, T., Norford, L., 2018. Urban Climate Numerical modeling of outdoor thermal comfort in 3D. Urban Climate 26, 212–230.

Nice, K. A., 2016. Development, validation, and demonstration of the VTUF-3D v1.0 urban micro-climate model to support assessments of urban vegetation influences on human thermal comfort. Phd thesis, Monash University.

Nice, K. A., Coutts, A. M., Tapper, N. J., 2018. Development of the VTUF-3D v1.0 urban micro-climate model to support assessment of urban vegetation influences on human thermal comfort. Urban Climate 24, 1052–1076.

Nicholls, N., Skinner, C., Loughnan, M., Tapper, N., 2008. A simple heat alert system for Melbourne, Australia. International Journal of Biometeorology 52 (5), 375–84.
URL http://www.ncbi.nlm.nih.gov/pubmed/18058138

Oke, T., 1982. The energetic basis of the urban heat island. Quarterly Journal of the Royal Meteorological Society 108, 1–24.
URL http://onlinelibrary.wiley.com/doi/10.1002/qj.49710845502/abstract

Peng, W., Wang, R., Duan, J., Gao, W., Fan, Z., 2022. Surface and canopy urban heat islands: Does urban morphology result in the spatiotemporal differences? Urban Climate 42, 101136.
URL https://doi.org/10.1016/j.uclim.2022.101136

Perkins-Kirkpatrick, S. E., Lewis, S. C., 2020. Increasing trends in regional heatwaves. Nature Communications 11 (3357).
URL http://dx.doi.org/10.1038/s41467-020-16970-7

Potgieter, J., Nazarian, N., Lipson, M. J., Hart, M. A., Ulpiani, G., Morrison, W., Benjamin, K., 2021. Combining High-Resolution Land Use Data

With Crowdsourced Air Temperature to Investigate Intra-Urban Microclimate. Frontiers in Enviromental Science 9, 720323.

Puliafito, S. E., Bochaca, F. R., Allende, D. G., Fernandez, R., 2013. Green Areas and Microscale Thermal Comfort in Arid Environments: A Case Study in Mendoza, Argentina. Atmospheric and Climate Sciences 2013, 372–384.

Shobha, N., Asha, T., 2017. Monitoring Weather based Meteorological Data: Clustering approach for Analysis. In: 2017 International Conference on Innovative Mechanisms for Industry Applications (ICIMIA).

Skarbit, N., Stewart, I. D., Ungera, J., Gál, T., 2017. Employing an urban meteorological network to monitor air temperature conditions in the local climate zones' of Szeged, Hungary. International Journal of Climatology 37, 582–596.

Solcerova, A., van Emmerik, T., Hilgersom, K., van de Ven, F., van de Giesen, N., 2018. Uchimizu: A Cool(ing) Tradition to Locally Decrease Air Temperature. Water 10 (741).

Stewart, I. D., Krayenhoff, E. S., Voogt, J. A., Lachapelle, J. A., Allen, M. A., Broadbent, A. M., 2021. Time Evolution of the Surface Urban Heat Island. Earth's Future 9, e2021EF002178.

Stewart, I. D., Oke, T. R., Krayenhoff, E. S., 2014. Evaluation of the local climate zone' scheme using temperature observations and model simulations. International Journal of Climatology 34, 1062–1080.

Top, S., Milosevic, D., Caluwaerts, S., Hamdi, R., Savic, S., 2020. Intra-urban differences of outdoor thermal comfort in Ghent on seasonal level and during record-breaking 2019 heat wave. Building and Environment 185, 107103.

Verdonck, M.-L., Demuzere, M., Hooyberghs, H., Beck, C., Cyrys, J., Schneider, A., Dewulf, R., Van Coillie, F., 2018. The potential of local climate zones maps as a heat stress assessment tool, supported by simulated air temperature data. Landscape and Urban Planning, 183–197.
URL https://doi.org/10.1016/j.landurbplan.2018.06.004

Yang, X., Yao, L., Jin, T., Peng, L. L. H., Jiang, Z., Hu, Z., Ye, Y., 2018. Assessing the thermal behavior of different local climate zones in the Nanjing metropolis, China. Building and Environment 137, 171–184.
URL https://doi.org/10.1016/j.buildenv.2018.04.009

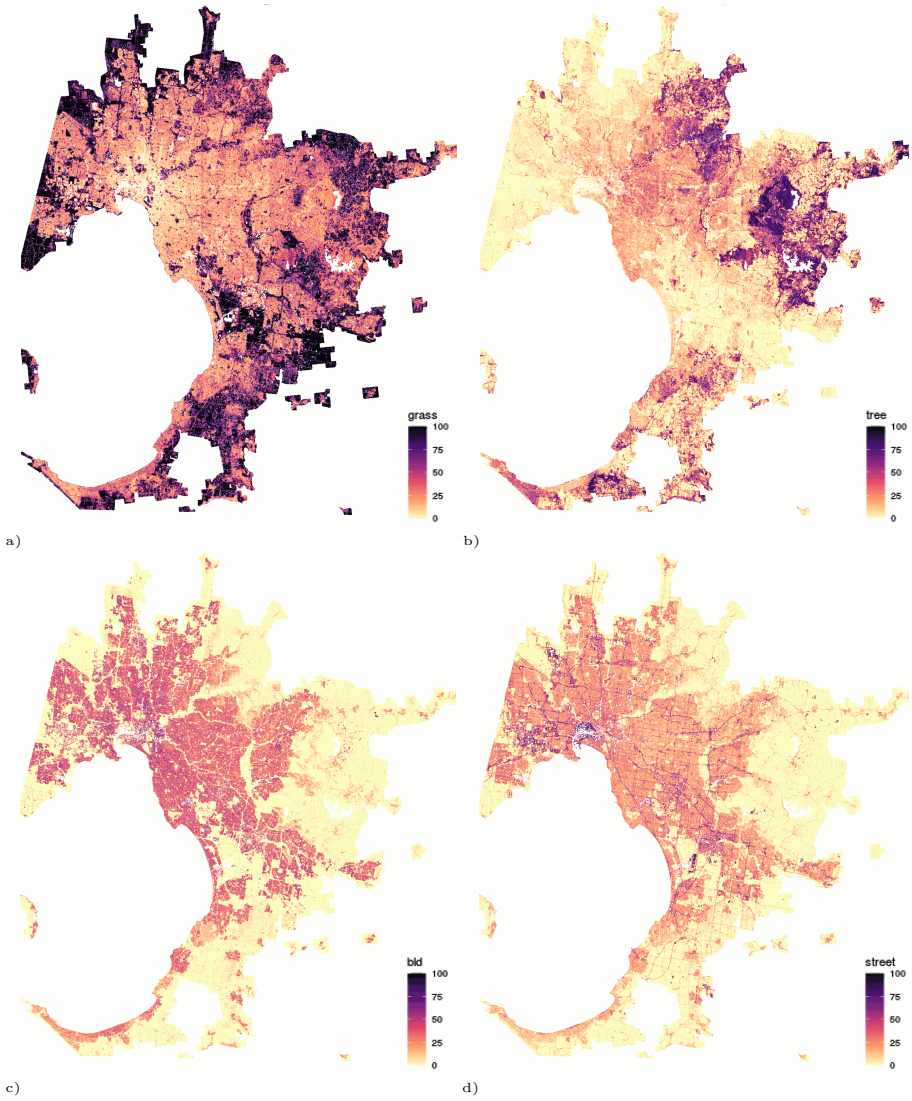

Figure S1: **Surface fractions (in percentages) of a) grass, b) trees, c) buildings, and d) streets across Melbourne.**

7. Acknowledgements

KAN is supported by NHMRC/UKRI grant (1194959).

8. Supplementary Figures

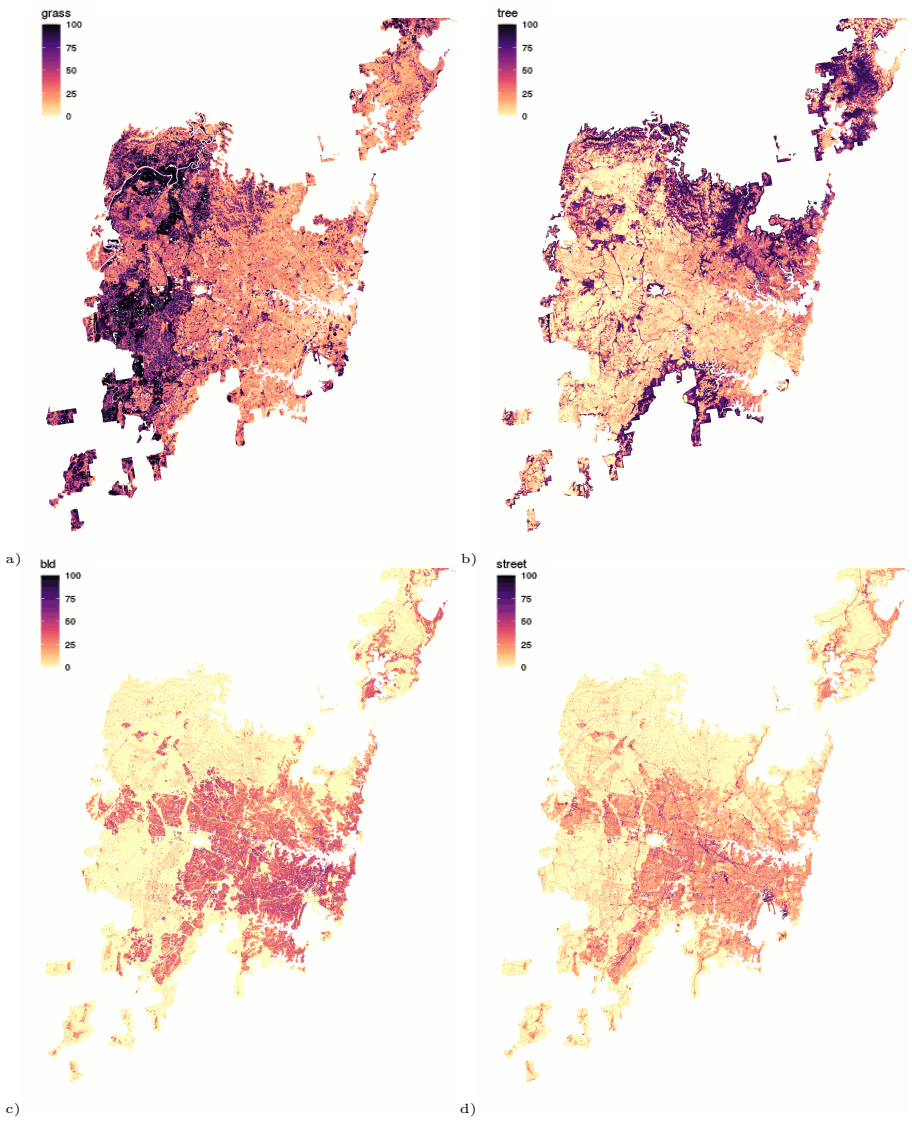

Figure S2: **Surface fractions (in percentages) of a) grass, b) trees, c) buildings, and d) streets across Sydney.**

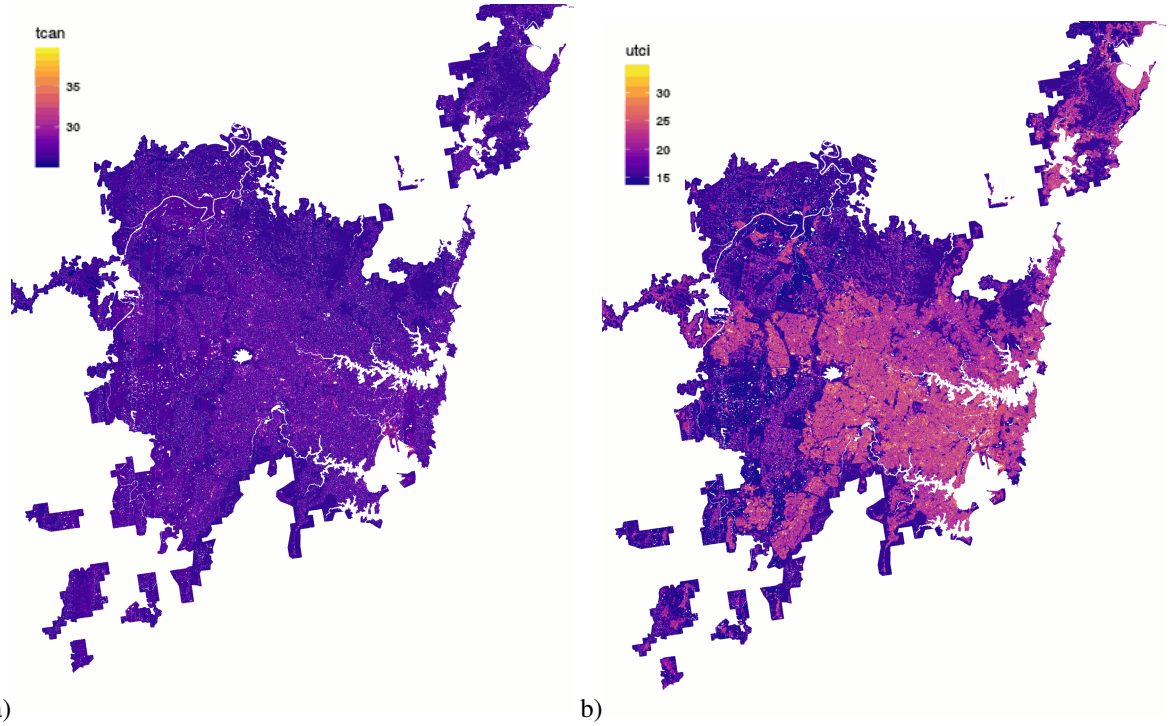

Figure S3: **a)** T_{can} **and b)** $UTCI$ **heatmaps on February 12, 2004 at 2pm generated by matching the closest matching parameters of surface fractions and average heights for each 100×100m location in Sydney from 9814 modelled scenario results (in** °C**).**

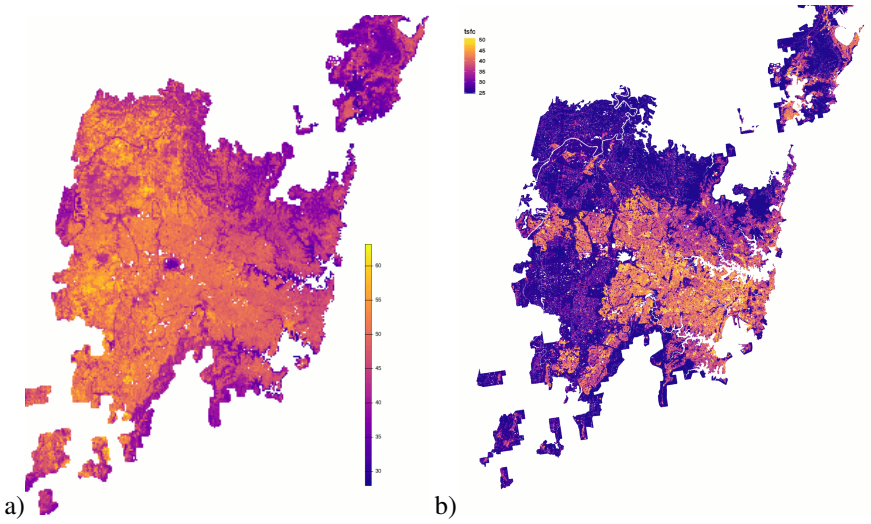

Figure S4: **a) Landsat 8 land surface temperature** (°C) **captured 10am March 11, 2019. Local conditions of air temperature on this day were minimum and maximum of 22 and 26**°C**. b) Modelled** T_{sfc} (°C) **on February 12, 2004 at 10am generated by matching the closest matching parameters of surface fractions and average heights for each 100×100m location in Sydney from 9814 modelled scenario results.**

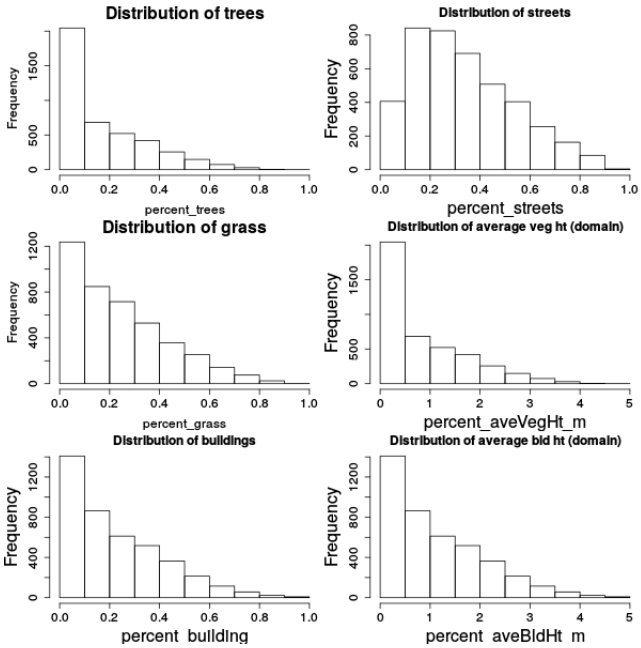

Figure S5: **Distribution of surface types across all modelled scenarios.**